


FULL PAPER

Open Access



Investigation of geomagnetic reference models based on the Iridium[®] constellation

Samuel Califf^{1,2*} , Patrick Alken^{1,2}, Arnaud Chulliat^{1,2}, Brian Anderson³, Kenneth Rock⁴, Sarah Vines³, Robin Barnes³ and Kan Liou³

Abstract

The World Magnetic Model (WMM) is a geomagnetic main field model that is widely used for navigation by governments, industry and the general public. In recent years, the model has been derived using high accuracy magnetometer data from the Swarm mission. This study explores the possibility of developing future WMMs in the post-Swarm era using data from the Iridium satellite constellation. Iridium magnetometers are primarily used for attitude control, so they are not designed to produce the same level of accuracy as magnetic data from scientific missions. Iridium magnetometer errors range from 30 nT quantization to hundreds of nT errors due to spacecraft contamination and calibration uncertainty, whereas Swarm measurements are accurate to about 1 nT. The calibration uncertainty in the Iridium measurements is identified as a major error source, and a method is developed to calibrate the spacecraft measurements using data from a subset of the INTERMAGNET observatory network producing quasi-definitive data on a regular basis. After calibration, the Iridium data produced main field models with approximately 20 nT average error and 40 nT maximum error as compared to the CHAOS-7.2 model. For many scientific and precision navigation applications, highly accurate Swarm-like measurements are still necessary, however, the Iridium-based models were shown to meet the WMM error tolerances, indicating that Iridium is a viable data source for future WMMs.

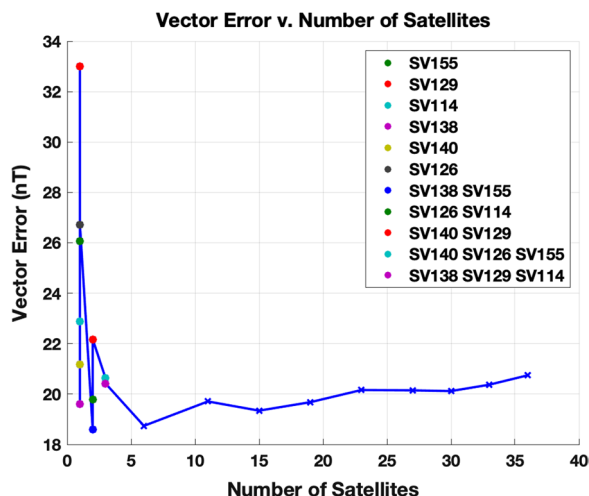
Keywords: Geomagnetism, Main field modeling, Constellation, Magnetometer

*Correspondence: califf@colorado.edu

¹ Cooperative Institute for Research in Environmental Sciences, University of Colorado, Boulder, USA

Full list of author information is available at the end of the article

Graphical Abstract



Introduction

The Earth’s core produces a large-scale magnetic field that is the dominant signal as measured by magnetometers on the surface of the Earth and in low-Earth orbit. Main field models such as the International Geomagnetic Reference Field (IGRF) (Alken et al. 2021b) and World Magnetic Model (WMM) (Chulliat et al. 2021), are used as references for navigation purposes, with applications ranging from aviation maps to spacecraft attitude control. These models include contributions from the slowly varying core field and the lithospheric field, which is assumed to be relatively static. The models are typically updated every 5 years to account for temporal changes in the core field, and a linear secular variation forecast is included to estimate the field for the next 5 years.

Beginning with the launch of Oersted and CHAMP in 1999–2000, satellite magnetometer data have played a critical role in IGRF and WMM models. The more recent models have relied on data from Swarm, which consists of three spacecraft in 460–510 km orbits with 87° inclination, and the vector magnetic field measurements are accurate to approximately 1 nT (Friis-Christensen et al. 2006). Each Swarm satellite carries a triaxial fluxgate magnetometer and an absolute scalar magnetometer, which is used as a reference to perform a scalar calibration of the fluxgate. Magnetic fields generated by spacecraft systems are mitigated in the magnetic measurements by mounting the magnetometers on a 4 meter boom. Also, significant effort was required to identify and remove additional error signals discovered after launch that were attributed to thermoelectric currents near the magnetometers (Tøffner-Clausen et al. 2016). The

motivation of this study is to evaluate the Iridium constellation as a potential data source for future main field models in the post-Swarm era.

The Iridium communications network consists of 66 satellites spread across 6 orbit planes that are equally spaced in local time. The first generation of Iridium satellites, Block 1, were launched between 1997 and 2002. This study focuses on the Iridium NEXT constellation, which was launched beginning in 2017 to replace the older Block 1 constellation. The entire Iridium NEXT constellation (66 operational satellites and 9 spares) has been launched and is currently operating, and data for all satellites have been processed with on-orbit corrections for satellite-generated magnetic field contamination. These corrections are a first version compensation for spacecraft signals and the corrections continue to be improved. This study uses an earlier version of the magnetometer data from 36 satellites to assess the feasibility of applying Iridium NEXT data for main field characterization. From a sampling perspective, the Iridium constellation is ideal for main field modeling due to its excellent spatial and temporal coverage of the Earth’s magnetic field. However, the magnetometers were intended for attitude control, and the measurements are much less accurate than those provided by a Swarm-like scientific mission.

Iridium satellites feature body-mounted triaxial fluxgate magnetometers, and nearby spacecraft components can contribute large (up to hundreds of nT) contamination signals. The Iridium NEXT satellites were not calibrated for magnetic contamination prior to launch. Hence, an extensive analysis effort was undertaken by

JHU/APL and Iridium to identify spacecraft contamination sources via correlation with housekeeping telemetry and perform on-orbit correction of each source to provide a data set as free as possible from spacecraft-generated magnetic fields. The sources and their corrections vary between the 75 Iridium NEXT satellites, every source from each satellite is corrected individually, and the data processing uses fully automated correction algorithms. A detailed discussion of the Iridium NEXT correction process and results is in preparation.

Unlike Swarm, Iridium satellites do not carry scalar magnetometers to use for calibrating the fluxgate measurements. Fluxgate magnetometers are susceptible to thermal variations and other error sources that can cause changes in the bias, scale factor, alignment and non-orthogonality calibration parameters (Olsen et al. 2003). Small errors in calibration parameters can result in relatively large measurement errors. For example, in a 50,000 nT field, a 100 nT error can be generated by a 0.2% scale factor error or a 0.1° alignment error. Due to the nature of the high-inclination orbit and the nadir-pointing attitude mode, measurement errors arising from inaccurate calibration in the spacecraft frame have a systematic component that maps to geographical location. Therefore, calibration errors are not zero-mean in the Earth-fixed frame and can have a larger impact on the model accuracy than random noise in the measurements.

A key component of this work is to calibrate the Iridium measurements without relying on existing models of the field or data from Swarm-like spacecraft missions, as the goal is to evaluate whether Iridium is a viable alternative to Swarm for future main field models. The standard AMPERE data product uses a main field reference model to linearly calibrate the data, and the residuals between the calibrated measurements and the reference model are reported. The purpose of AMPERE is to measure time-varying magnetic fields caused by Birkeland currents (Anderson et al. 2000, 2021) rather than to measure the main field itself. In this study we use a version of the Iridium magnetometer data that has been corrected for spacecraft contamination signals, but has not been calibrated relative to a reference model. We then calibrate the Iridium data relative to model derived from a subset of the INTERMAGNET global observatory network producing quasi-definitive (QD) data (Peltier and Chulliat 2010) on a regular basis. Quasi-definitive data are data corrected using provisional baselines, produced soon (less than 3 months) after their acquisition, and very close (less than 5 nT difference) to the observatory definitive data product (<https://www.intermagnet.org/>

faqs-eng.php). This is to be compared with the typical delay of 6–12 months (sometimes much longer) in distributing definitive data at most observatories.

The “[Main field inversion](#)” section provides an overview of the main field modeling process. The Iridium orbital configuration, data and corrections for spacecraft contamination are discussed in the “[Iridium NEXT data](#)” section. Iridium measurement characteristics are presented in the “[Iridium NEXT data quality](#)” section, demonstrating the need to constrain the calibration parameters. In the “[Calibration model from observatories](#)” section, a main field model is derived from quasi-definitive observatory data that is later used to calibrate the Iridium measurements. The “[Iridium NEXT main field models](#)” section presents the model results for a 2018 main field model using Iridium data, and the “[Effect of increasing number of satellites](#)” section explores the impact of increasing the number of satellites used in the model inversion. The “[Conclusions](#)” section summarizes the study.

Main field inversion

We follow standard practices in building geomagnetic main field models from both satellite and ground observatory data sets using software developed for the World Magnetic Model at the National Centers for Environmental Information (NCEI). The modeling process is described in detail in Alken et al. (2020). We briefly review the main ideas used to fit main field models to a set of scattered observations. We assume that no electric currents flow in the observation region, so that the magnetic field can be represented as the gradient of a potential field, $\mathbf{B} = -\nabla V$, with

$$V(r, \theta, \phi, t) = a \sum_{n=1}^N \sum_{m=-n}^n g_n^m(t) \left(\frac{a}{r}\right)^{n+1} S_n^m(\theta, \phi) \quad (1)$$

where (r, θ, ϕ) are the radius, co-latitude and longitude, respectively, in a geocentric spherical coordinate system, t is time, $a = 6371.2$ km is a reference radius, and N is the maximum spherical harmonic (SH) degree. The $g_n^m(t)$ are the Gauss coefficients which describe both the temporal and spatial structure of the field, and

$$S_n^m(\theta, \phi) = \begin{cases} \cos(m\phi)P_n^m(\cos\theta), & m \geq 0 \\ \sin(|m|\phi)P_n^{|m|}(\cos\theta), & m < 0 \end{cases} \quad (2)$$

where $P_n^m(\cos\theta)$ are the Schmidt semi-normalized associated Legendre functions. The time dependence of the Gauss coefficients $g_n^m(t)$ is typically parameterized with

a spline representation, which is defined as piecewise polynomials between chosen knot intervals. However, due to the significant noise present in the Iridium data, we found that higher degree polynomials are not well constrained in the inversion, and so we restrict the $g_n^m(t)$ to be simply linear in t over the full time interval of the model inversion.

To fit the above model to a data set, we define a cost function to be minimized in a least-squares sense:

$$\chi^2 = \sum_{i=1}^{N_\epsilon} w_i \|\epsilon_i\|^2 + \lambda^2 \mathbf{c}^T \Lambda \mathbf{c} \quad (3)$$

The residuals ϵ_i refer to Iridium vector magnetic field measurements rotated to a geographic Earth-fixed reference frame using a set of Euler rotation angles, and reduced by the internal field model described above see Alken et al. ([2020, Eq. 37]). N_ϵ is the number of residuals, and w_i is a weight assigned to each residual. The weights are determined by a robust Huber iterative re-weighting scheme to reduce the effect of outliers, and spacecraft data are also weighted by spatial location to account for the increased sampling at high latitudes by high-inclination orbits. The coefficient vector \mathbf{c} contains the Gauss coefficients as well as the Euler angles. The matrix Λ is a regularization condition which is discussed in more detail in the sections below. Full details concerning the Euler angles, data weighting, and minimization procedure can be found in (Alken et al. 2020). Magnetometer calibration parameters are often co-estimated with the Gauss coefficients. Given the challenge of constraining the Iridium calibration with a sparse ground observatory network, we chose to separate the process into three steps. First, we develop a SH degree 12 main field model using ground-based observatory data, and then calibrate the Iridium data daily relative to the observatory model evaluated to SH degree 8. Finally, we invert the pre-calibrated Iridium data to produce a SH degree 12 main field model.

Iridium NEXT data

This study uses magnetometer data from the Iridium NEXT constellation, which is the second generation of Iridium satellites. There are 66 satellites in the Iridium communications network in 778 km altitude circular orbits with 86.4° inclination. The satellites are distributed with 11 satellites in each of 6 orbit planes evenly spaced in longitude with nominal 2-h local time separations. The Iridium NEXT magnetometers are sampled every 8 s, so that the full constellation samples Earth's magnetic field globally every 2 h with 2.3° resolution in longitude and 0.5° resolution in latitude.

The fluxgate magnetometer provides a vector measurement of the magnetic field every 8 s. Corrections for spacecraft-generated fields are applied in satellite body coordinates before rotating into inertial coordinates. These measurements are first rotated into Earth Centered Inertial (ECI) coordinates using pointing information from the attitude determination system (Hapgood 1992), and then converted to geographic North–East–Center (NEC) coordinates for main field modeling. Iridium NEXT uses star cameras for attitude determination with an attitude knowledge uncertainty of 0.02°, which is a significant improvement over the 0.2° attitude uncertainty for the previous Block 1 constellation that did not have star cameras. The magnetometer measurements are quantized to 30 nT, and the departures of on-orbit magnetometer scale factors, offsets, and orthogonality, relative to the magnetometer manufacturer specifications, together with uncertainties in the spacecraft field corrections combine with the attitude errors to produce the overall uncertainty.

Iridium magnetometer data are acquired for scientific purposes for the Active Magnetosphere and Planetary Electrodynamics Response Experiment (AMPERE, <http://ampere.jhuapl.edu>) through the NSF Geospace facilities program. This study leverages data acquired under AMPERE-II and AMPERE-3 which supported the acquisition and calibration of data from the Iridium NEXT satellites. The derivation of the corrections and the continued spacecraft contamination correction assessment and upgrades are supported under AMPERE. For standard AMPERE processing, the data are calibrated against a reference model after removing the vehicle contamination signals (cf. Anderson et al. 2021). However, for this analysis, a custom data product was generated which is corrected for spacecraft-generated fields but which has not been calibrated against a reference model. Thus, the data all use the same scale factors for all axes of all magnetometers and assume zero offsets and perfect alignment/orthogonality. From the AMPERE processing it is known that the relative scale factors, offsets, and orthogonality deviate substantially from these ideal assumptions. Nonetheless, using this entirely uncalibrated starting point is essential to produce independent main field models that do not depend on prior knowledge of the field. These data for all Iridium NEXT satellites have been generated. For this study, we focus on data from a subset of 36 satellites for the time period from 2018-03-01 through 2019-04-29, because this subset was the earliest available.

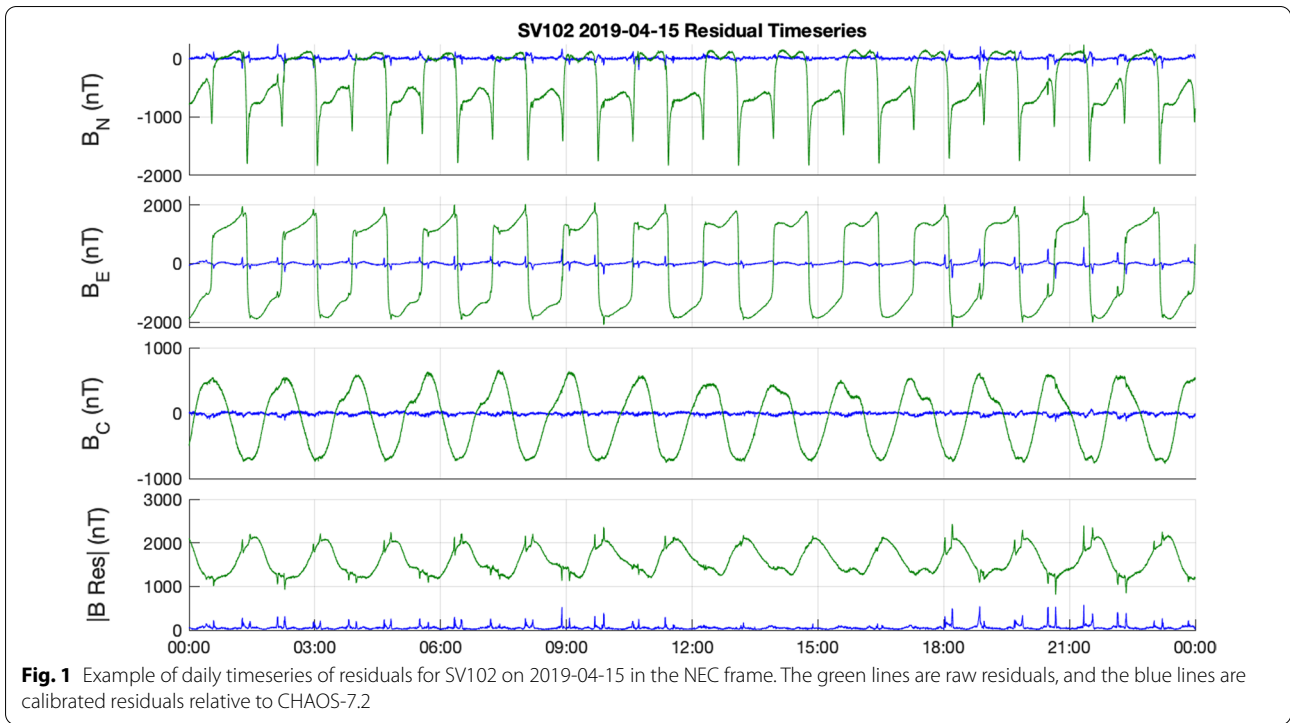


Fig. 1 Example of daily timeseries of residuals for SV102 on 2019-04-15 in the NEC frame. The green lines are raw residuals, and the blue lines are calibrated residuals relative to CHAOS-7.2

Iridium NEXT data quality

An example of Iridium NEXT residuals for space vehicle (SV) 102 on 2019-04-15 is shown in Fig. 1. The residuals are computed relative to the CHAOS-7.2 main field model (Finlay et al. 2020) up to spherical harmonic degree 15 and MF7 crustal field (Maus et al. 2008) (SH degrees 16–133). The raw measurements (green line) include corrections for known spacecraft contamination signals, but no on-orbit linear calibration has been applied. The uncalibrated measurements have large errors (>1000 nT), and the data cannot be directly inverted to produce a reasonable main field model. Calibration errors create systematic errors with orbital periods that are larger than the random noise in the data, so constraining the calibration is a critical step to the modeling effort. For initial residual analysis, we calibrate the data relative to the CHAOS-7.2 main field model (SH degrees 1–15) and MF7 crustal field (Maus et al. 2008) (SH degrees 16–133). We use a linear calibration given by

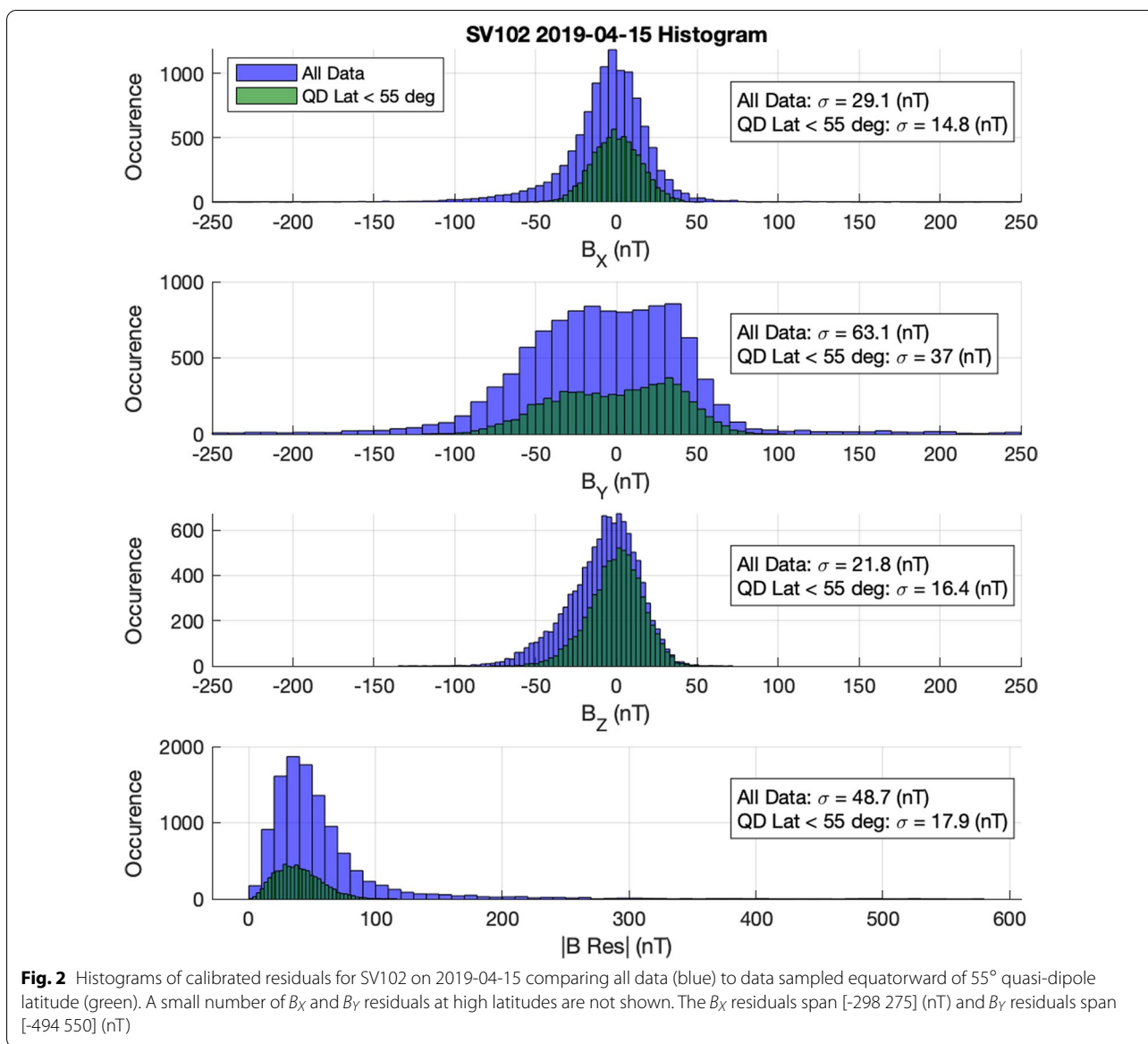
$$\mathbf{B}_{cal} = \mathbf{A}\mathbf{B}_{meas} + \mathbf{O} \tag{4}$$

where \mathbf{B}_{cal} is the calibrated measurement in the star camera frame and \mathbf{B}_{meas} is the uncalibrated measurement in the instrument frame. The \mathbf{A} matrix elements specify the 3 scale factors, 3 non-orthogonality angles, and 3 alignment angles between the instrument and star camera

frames. The vector \mathbf{O} contains the 3 biases. The calibration parameters can be extracted from the \mathbf{A} matrix as described in Alken et al. (2020). The \mathbf{A} and \mathbf{O} parameters are derived by a least squares linear fit to CHAOS-7.2 and MF7. Data are restricted to quasi-dipole latitudes (QDLat) below 55° (Richmond 1995) for calibration to reduce the influence of field aligned currents at high latitudes.

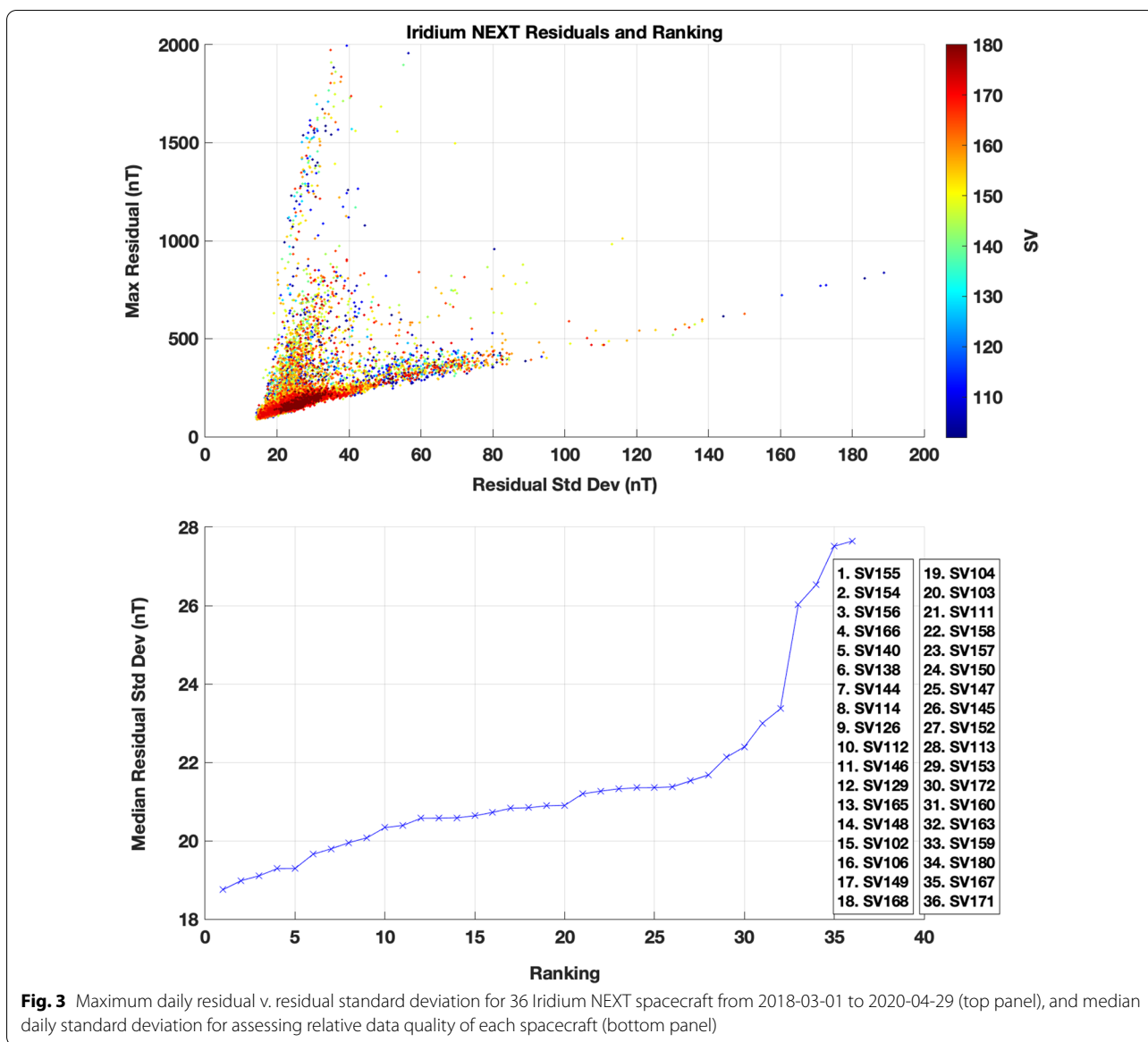
After calibration the residuals are significantly reduced. The spikes that remain in the calibrated residuals are high-latitude external fields that are not included in the reference model. (We note in passing that these spikes are the signatures of Birkeland currents which are the basis for AMPERE science products.) Pre-calibration is a critical step to producing a main field model, and for future models, we cannot rely on prior knowledge of the field from Swarm-based models, such as CHAOS. We address this by introducing a calibration model derived from quasi-definitive observatories in the “[Calibration model from observatories](#)” section.

Figure 2 displays histograms of the calibrated residuals corresponding to the timeseries example in Fig. 1. The residuals are expressed in the spacecraft frame, where Z points toward geodetic nadir, Y is anti-aligned with the orbit normal vector and X is approximately along the spacecraft velocity direction. The variation is largest in



the spacecraft Y component, which points westward for ascending orbits and eastward for descending orbits. The magnetic field is mostly aligned in the radial and northward directions, so there is less change in the field along the spacecraft Y direction over the course of an orbit. This increases uncertainty in the spacecraft Y calibration relative to the XZ axes. The standard deviation of the residuals is smaller when the data are restricted to quasi-dipole latitudes below 55° because of the increased variation in the magnetic field at high latitudes related to field-aligned currents and other external fields. Therefore, we use the low-latitude residuals to assess the quality of the measurements from each spacecraft.

A summary of the daily residuals for all 36 Iridium NEXT spacecraft used here is shown in Fig. 3 (top panel), where the residual is defined as the magnitude of the calibrated vector residual. The maximum residual is plotted against the standard deviation of residuals for each day, and the color indicates the spacecraft vehicle identification number. Most of the distribution lies between 20–40 nT standard deviation and 150–300 nT maximum residual. There is a “V” shaped distribution, where the left side of the “V” reflects days, where the residuals are generally small with a few large outliers. These outliers are addressed in the modeling process by applying robust Huber weighting. The right side



of the “V” indicates days where the measurements are generally more disturbed relative to the reference main field model, either by real variations in the magnetic field related to geomagnetic activity or by increased contamination from the spacecraft. Prior to creating a model, geomagnetically active days were removed as part of the standard data selection process, and days where the data are known to be affected by spacecraft operations were identified by JHU-APL/Iridium and removed from the data set. The medians of daily residual standard deviations for each spacecraft were used as a metric to rank the quality of the data (Fig. 3 bottom

panel). For most of the spacecraft, the median standard deviation is between 18–24 nT, and 4 of the spacecraft have slightly larger measurement errors. The ranking is used to construct models with subsets of the constellation to explore the effect of measurement quality and orbit plane selection on the main field model accuracy in the “Effect of increasing number of satellites” section.

Figure 4 shows the variation in the calibration parameters for SV126 over the duration of the data set. The calibration parameters were computed daily relative to CHAOS-7.2 and MF7 using Eq. 4. There are large, rapid changes in the biases of several hundred nT during

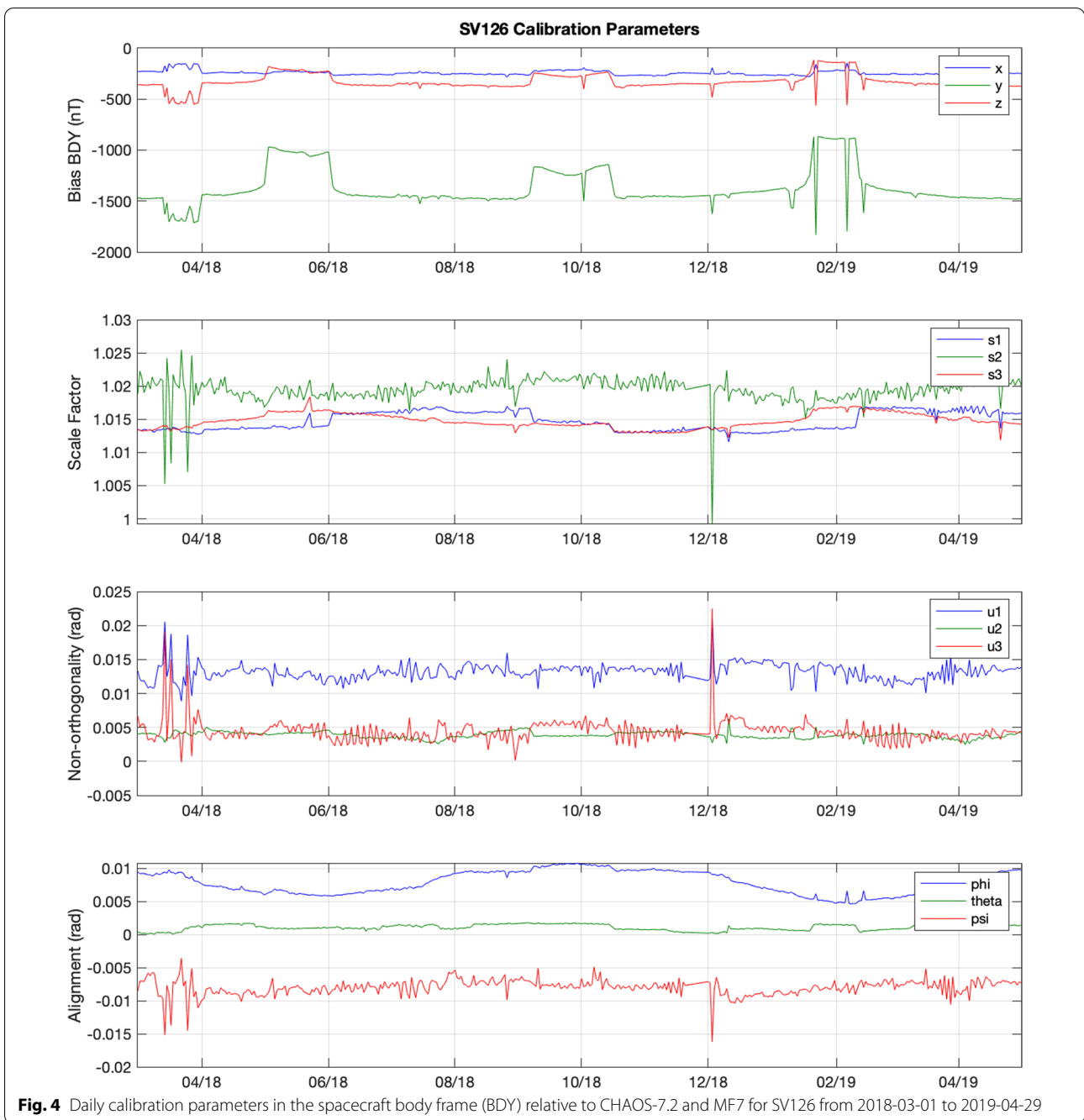
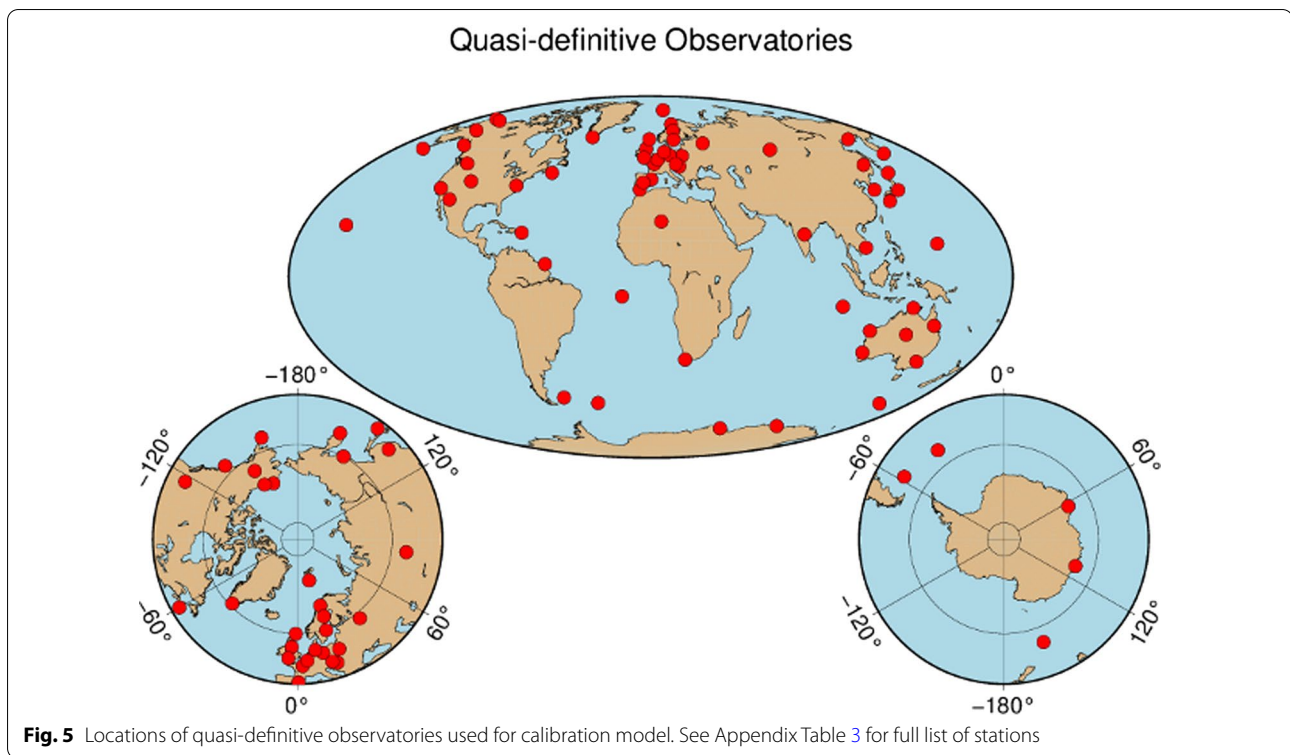


Fig. 4 Daily calibration parameters in the spacecraft body frame (BDY) relative to CHAOS-7.2 and MF7 for SV126 from 2018-03-01 to 2019-04-29

certain times of year, which are likely related to power system adjustments related to the beta angle. The scale factor, non-orthogonality and alignment parameters are more stable. The spikes may be related to operational events on the spacecraft and unmodeled external fields during geomagnetic storms. Given the timescale of the

bias variations, we chose to calibrate the data daily as a first step in the modeling process, rather than co-estimate calibration parameters with the Gauss coefficients using monthly splines. To maintain independence from other satellite measurements, we calibrate the data relative a main field model derived from observatories.



Calibration model from observatories

Overview

To evaluate Iridium NEXT as a primary data source for producing future main field models, we must calibrate the data without using main field models derived from low-Earth orbit satellite data, such as CHAOS or IGRF. Our approach is to first construct a main field model using data from a set of observatories producing quasi-definitive data on a regular basis, and then calibrate the Iridium data using the observatory model. The pre-calibrated Iridium data are then used to derive the final model.

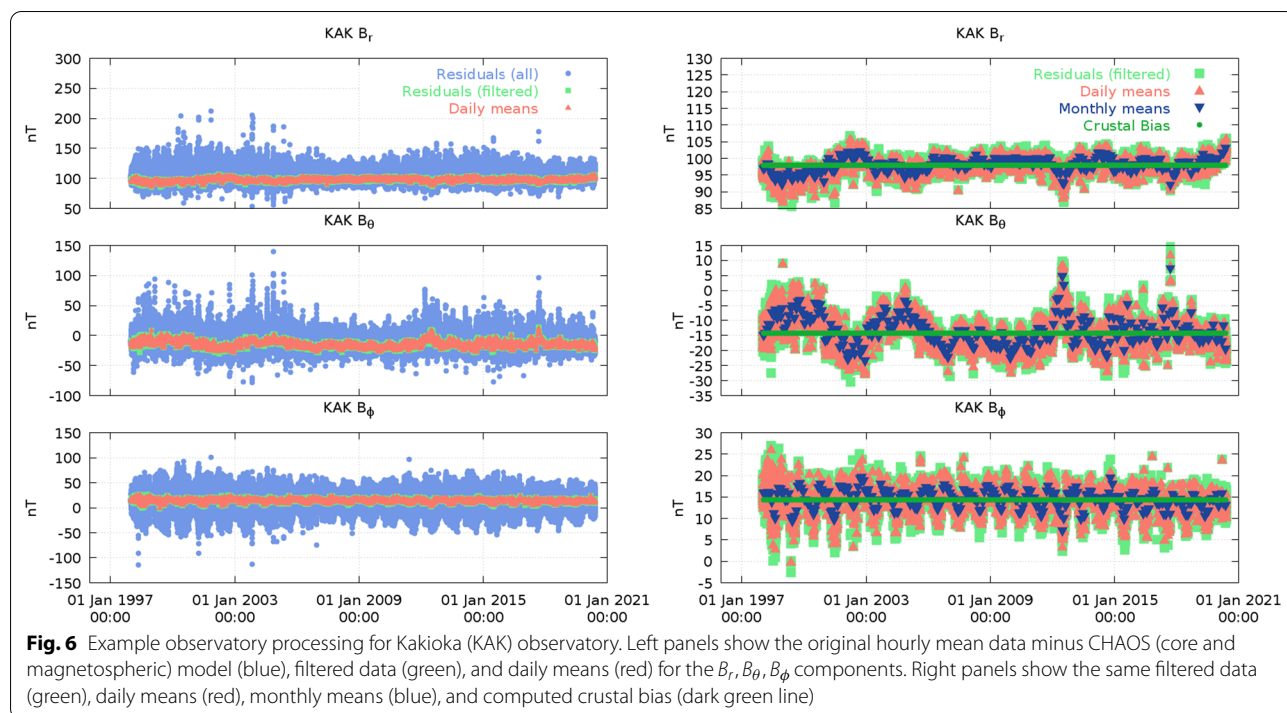
We restrict our analysis to observatories able to produce quasi-definitive data, because in the post-Swarm era Iridium data would need to be calibrated as soon as possible after being collected. Specifically, we select a subset of 59 INTERMAGNET observatories, which have historically shown that they are reliable in producing quasi-definitive data within about 6 months. A map of the 59 quasi-definitive observatories is shown in Fig. 5, and the full list is given in Appendix Table 3.

For each observatory, we start from the hourly mean data compiled by Macmillan and Olsen (2013), which is based primarily on the data provided by the

observatories, with additional processing steps to quality control the data and prepare them for use in geomagnetic main field modeling (e.g., correct data discontinuities, convert all data to geographic spherical components and coordinates). We select the hourly mean data for geomagnetically quiet conditions using the criteria:

- Local time of measurement between 01:00 and 05:00 A.M.
- Kp index less than 3
- Temporal change of RC index (Olsen et al. 2014), $|dRC/dt|$ does not exceed 4 nT/h.
- Interplanetary magnetic field (IMF) B_z component between 0 and 6 nT
- IMF B_y component between -6 and 6 nT

After the data are selected for each station according to these criteria, we compute the mean value of all remaining hourly values for each day, which we then call daily means. An example is shown in the left panels of Fig. 6 for the Kakioka station (KAK). The left panels show the original hourly mean data after removing the CHAOS-7.2 (Finlay et al. 2020) main field and external field models in blue, the filtered residuals in green, and the daily



mean residuals in red. The variance of the filtered (green) data is significantly reduced relative to the variance of the original data, which is primarily caused by magnetic field perturbations originating in the ionosphere and magnetosphere. These daily mean time series primarily represent the internal main field plus an unknown crustal bias due to magnetized rocks in Earth’s crust in the vicinity of the observatory. Since the reference model (CHAOS) is built mainly from satellite data, for which accurate crustal models already exist, we can estimate the crustal bias for each station by simply analyzing the daily mean residuals with respect to spherical harmonic degrees 1 to 15 of CHAOS over the past 20 years (2000–2020) when high-resolution data from CHAMP and Swarm are available. We argue that using CHAOS in this manner is appropriate, since crustal biases do not change significantly over long time periods. By computing the crustal biases of the quasi-definitive stations in the CHAMP/Swarm era, we expect to be able to use those values long into the future. This method, however, would not work if a new observatory is installed after Swarm is decommissioned. In the right panels of Fig. 6, we again plot the filtered residuals (green), daily mean residuals (red), and additionally the monthly mean residuals (blue) for each field component. We then calculate the crustal bias of each component as the median value of the daily mean residuals, taken over a 20-year time period. These crustal biases are shown as green horizontal lines in the figure. For the KAK station,

these biases are less than 100 nT in magnitude, however for other stations they can reach hundreds of nT, depending on the location of the observatory. The full set of estimated crustal biases are provided in Table 3. A comparison of our crustal bias values with the recent study of Verbanac et al. (2015) reveals that many of our values are within 2- σ error bars as reported by that study. Some stations have larger discrepancies which we are currently unable to explain, although Verbanac et al. (2015) used different models of the core and external field to process their data, as well as a different time period which could contribute to the observed differences. A detailed comparison of our crustal bias estimates with previous studies is beyond the scope of the present work.

Main field modeling from the observatory network

Building main field models from the observatory network differs from satellite models in that we need to account for the large spatial gaps, primarily located in the oceanic regions. Left untreated, these large spatial gaps could produce thousands of nT error in the fitted model. Therefore, we need to employ slightly different regularization strategies to prevent the fitted model from oscillating wildly in these gap regions. Numerous regularization norms have been proposed over the years, which are based on both physical principles and empirical observations. We considered three norms for our model: the minimum energy

norm (Shure et al. 1982), the norm which minimizes the rms of B_r over the core mantle boundary (CMB) (Shure et al. 1982), and the minimum curvature of B_r over the CMB (Smith and Wessel 1990). We experimented with all three of these regularization norms, and found that the resulting models all performed similarly in the observatory gap regions. In all cases, the model error (compared to the unregularized solution) was significantly reduced. We could not identify a clearly superior regularization strategy, so we opted to use the minimal B_r rms condition for our final model, which is widely used in satellite based main field models, and minimizes the quantity:

$$M[\mathbf{B}] = \int dt \int_{S(c)} |B_r|^2 d\Omega \tag{5}$$

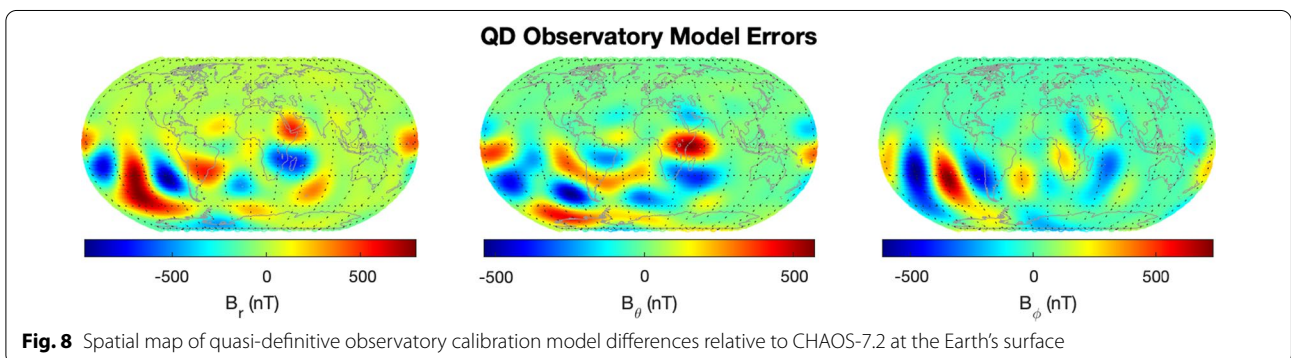
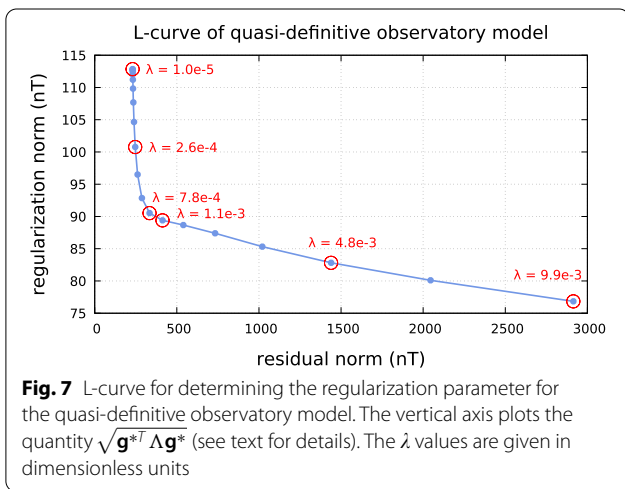
where $S(c)$ is a spherical shell of radius c , and $c = 3480$ km is the radius of the core mantle boundary.

We fit a spherical harmonic degree and order 12 internal geomagnetic field model to the quasi-definitive

observatory data set. To build a WMM in the post-Swarm era, we will need to determine the regularization parameter without relying on a prior model. To this end, we applied L-curve analysis to determine the optimal regularization parameter (Hansen and O’Leary 1993). The L-curve is a plot of the norm of the model residuals versus the norm of the regularized parameters, $\sqrt{\mathbf{g}^T \Lambda \mathbf{g}}$, where \mathbf{g} is the vector of Gauss coefficients, and Λ is the matrix representation of the regularization norm given in Eq. (5). In our study, $\Lambda = G \otimes C$, where G is the Gram matrix of the B-spline basis (Alken et al. 2020, Eq. 44), and C is a diagonal matrix given by

$$C_{nn',mm'} = 4\pi \left(\frac{a}{c}\right)^{2n+4} \frac{(n+1)^2}{2n+1} \delta_{mm'} \delta_{nn'} \tag{6}$$

Since the low spherical harmonic degree Gauss coefficients contain far more power than the high degree terms, the term $\sqrt{\mathbf{g}^T \Lambda \mathbf{g}}$ is dominated by the low-degree Gauss coefficients (in particular the dipole terms), and we found it difficult to identify a suitable regularization parameter with these terms included in the L-curve visualization. The low degree coefficients are well resolved by the quasi-definitive observatory network, even without regularization, and so for the purposes of visualization only, we opted to exclude SH degrees 1–7 from the solution norm used to plot the L-curve. Figure 7 presents the L-curve, in which the vertical axis represents the quantity $\sqrt{\mathbf{g}^{*T} \Lambda \mathbf{g}^*}$, and \mathbf{g}^* is the vector of Gauss coefficients for which SH degrees 1–7 are set to zero. We emphasize that all SH degrees 1–12 are regularized in the model fitting, but only SH degrees 8–12 are used to visualize the L-curve. This procedure allows us to select a regularization parameter λ which best constrains the high-degree terms, under the assumption that the low-degree terms are already well constrained by the observatory network. The optimal regularization parameter is chosen at the corner of the L-curve, corresponding approximately to



$\lambda = 10^{-3}$ (dimensionless units). This represents the value that provides sufficient regularization to minimize model errors associated with spatial gaps in the data while avoiding over-damping the model, which is reflected in the large residuals as the parameter is increased. We separately calculated the regularization parameter which provided the best spectral agreement between our quasi-definitive observatory model and CHAOS-7.2, and found the same value of $\lambda = 10^{-3}$. This demonstrates that we can construct observatory based models for calibrating Iridium using L-curve analysis without relying on prior models built from Swarm or other missions.

Figure 8 shows spatial difference maps between the quasi-definitive observatory model built with data between July 1, 2018 and July 31, 2020 and CHAOS-7.2 at the epoch 2018.0. We used linear Gauss splines to fit this roughly 2-year period to SH degree 12, and then extrapolated the coefficients back to 2018.0 for comparison with the CHAOS-7.2 model. The model was produced in reverse time order to evaluate the error over time relative to existing data, and the date range was selected to account for a potential 6-month delay in observatory data availability. The model has >500 nT errors in all components, and the largest errors generally correspond to areas with sparse observatory coverage in the southern hemisphere. We expect additional errors to arise from the fact that we cannot fully remove external fields and their induced counterparts (particularly at high-latitudes) from the observatory data, despite our careful data selection and pre-processing. However, we expect such errors to be far smaller than the errors arising from spatial data gaps in the observatory network, which appear dominant in Fig. 8. Given the lack of a simple analytical solution to the mapping between the calibration reference model error and the final inverted model accuracy, it is not immediately clear that this model is accurate enough to use as a calibration reference for Iridium measurements. In the following sections, we develop and evaluate models using Iridium data that have been pre-calibrated relative to this observatory model, and we demonstrate that this approach is capable of producing models that satisfy WMM error requirements.

Iridium NEXT main field models

Model description

We developed main field models to spherical harmonic degree 12 assuming linear secular variation for an epoch of 2018-01-01 using Iridium NEXT data from 2018-03-01 to 2019-04-29. IGRF and WMM models are produced using a data cutoff that is approximately 3 months

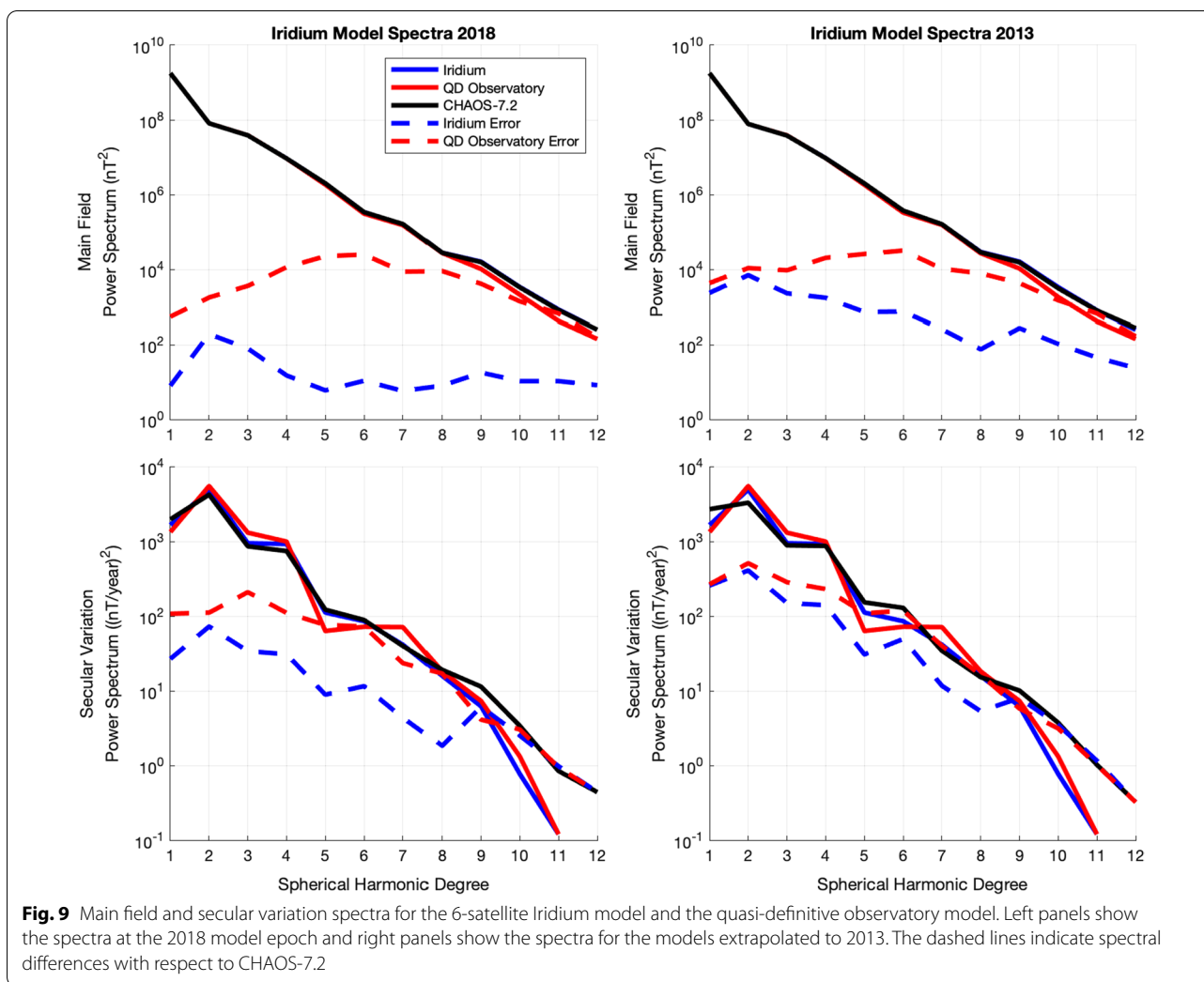
before the epoch, so this approach mimics the operational model production process in reverse. Similarly, the quasi-definitive observatory model for calibration uses data beginning on 2018-07-01 to account for a potential 6-month delay in the observatory data. To evaluate the model performance, we extrapolate the model backward in time to 2013 using the linear secular variation estimated at the 2018 epoch.

The Iridium data are pre-calibrated on a daily basis relative to the quasi-definitive observatory model developed in the “[Calibration model from observatories](#)” section. The quasi-definitive observatory model is truncated to spherical harmonic degree 8, as the observatories don’t provide reliable information on the higher order main field terms due to limited spatial sampling. The MF7 crustal field and CHAOS external field models are added to the quasi-definitive observatory main field model for the calibration reference field, although the crustal and external field terms are small relative to the errors in the quasi-definitive observatory model. This means we have a spectral gap for spherical harmonic degrees 9 through 15 in the model used to calibrate Iridium, since we have no available data sets to constrain these degrees. However, separate testing using the full CHAOS core field model for degrees 1 through 15 has shown that the calibration parameters change very little when including degrees 9 to 15 in the reference model. The calibration uses the linear fit described in the “[Iridium NEXT data quality](#)” section for data sampled equatorward of 55° quasi-dipole latitude.

We use standard criteria to select data during geomagnetically quiet periods to minimize the effect of external fields originating in the ionosphere and magnetosphere. These criteria are:

- Kp index does not exceed 2 for an entire orbit
- Temporal change of ring current (RC) index $|dRC/dt|$ does not exceed 3 nT/hour for an entire orbit
- Local time of ascending or descending node is between 22:00 and 05:00
- Interplanetary magnetic field (IMF) B_z component is between 0 and 6 nT
- IMF B_y component is between -6 and 6 nT
- For data poleward of $\pm 55^\circ$ quasi-dipole latitude, the Sun must be at least 10° below the horizon.

We also compute an along-track root mean square (rms) difference between the scalar field measured by Iridium and the quasi-definitive observatory model, and discard orbital tracks with an rms difference greater than 500 nT.



This is designed to detect and remove highly perturbed data from fields originating on the spacecraft. We additionally downsample the measurements of each spacecraft to 1 sample every 40 s. We also remove the MF7 crustal field model (SH degrees 16–133) (Maus et al. 2008) and the CHAOS external field model from the data to isolate the time-varying main field signal. To minimize the influence of field-aligned currents at high latitudes, we only use the radial component of the measurement poleward of 55° quasi-dipole latitude. Finally, main field models are computed from the pre-calibrated Iridium data using standard main field inversion techniques described in the “Main field inversion” section.

Model results

Figure 9 shows the main field and secular variation power spectra (Lowes 1966, 1974) for the quasi-definitive

observatory calibration model and a 6-satellite Iridium model derived using data that was pre-calibrated relative to the quasi-definitive observatory model. The best satellite from each plane was selected for the model based on the residual ranking described in the “Iridium NEXT data quality” section. Table 2 lists the spacecraft in order of residual ranking by orbit plane. The Iridium model was regularized by damping the first time derivative of the radial field component integrated over the CMB to reduce large and unphysical spectral power at higher degrees caused by measurement errors. We used L-curve analysis to choose the regularization parameter $\lambda_1 = 0.01$ (see Alken et al. 2020 for details), which causes the steep decay in the secular variation spectral power near SH degree 9.

The left panels in Fig. 9 show the spectra at the 2018 model epoch, and the right panels correspond to the

Table 1 Residual statistics for 6-satellite Iridium model

Spacecraft	Component	N	Mean (nT)	Sigma (nT)	rms (nT)
SV114	B_N	112108	-0.81	25.86	25.87
	B_E	112108	2.64	38.59	38.68
	Low B_C	112108	-2.82	27.09	27.24
	High B_C	36034	10.02	32.38	33.89
SV126	B_N	123807	-0.8	24.59	24.6
	B_E	123807	2.54	41.67	41.74
	Low B_C	123807	-2.34	25.25	25.36
	High B_C	36623	-2.08	30.68	30.75
SV129	B_N	121241	-0.43	24.76	24.77
	B_E	121241	3.17	41.45	41.58
	Low B_C	121241	-2.68	29.16	29.29
	High B_C	36283	-20.9	34.92	40.69
SV138	B_N	120138	-0.45	24.04	24.05
	B_E	120138	1.85	41.09	41.13
	Low B_C	120138	-2.45	24.73	24.85
	High B_C	36290	0.81	30.29	30.3
SV140	B_N	107206	-0.77	25.16	25.17
	B_E	107206	2.1	40.75	40.81
	Low B_C	107206	-2.97	24.61	24.79
	High B_C	33363	4.65	32.34	32.68
SV155	B_N	80594	-0.29	24.49	24.49
	B_E	80594	2.69	39.61	39.7
	Low B_C	80594	-2.31	25.08	25.19
	High B_C	26738	2.11	33.79	33.86

Magnetic field components are referenced to a North-East-Center coordinate system. Low-latitude refers to residuals equatorward of ± 55 quasi-dipole latitude. High-latitude refers to residuals poleward of ± 55 quasi-dipole latitude

end of the 5-year model interval in 2013. The 2013 model has been extrapolated backward in time using the secular variation estimated at the 2018 epoch. Initial errors in the linear secular variation estimate and non-linear changes in the core field cause the model error to increase over time. There is a significant improvement in both the main field and secular variation estimates using the calibrated Iridium data relative to the model derived from quasi-definitive observatories alone. The quasi-definitive observatory model has larger errors at all SH degrees, and the main field error power is a significant fraction of the total main field power above SH degree 8. This demonstrates that the Iridium data add valuable information about the main field, despite the fact that the Iridium calibration parameters depend on the quasi-definitive observatory model.

The Iridium model errors relative to CHAOS-7.2 at the Earth’s surface for the 2018 epoch are shown in the top panels of Fig. 10. At the model epoch, the maximum radial component errors are ~ 40 nT at high latitudes in both hemispheres, and the maximum B_θ and B_ϕ components errors are ~ 30 nT. The average error is approximately 20 nT. B_r and B_θ errors have a dominant low-order pattern with respect to latitude that corresponds to the spectral error peak at $n = 2$ in Fig. 9. This may be driven by calibration errors, as the calibration model has >500 nT errors (Fig. 8) and the calibration couples most strongly to the lower order model terms. The B_ϕ errors have a higher order longitudinal

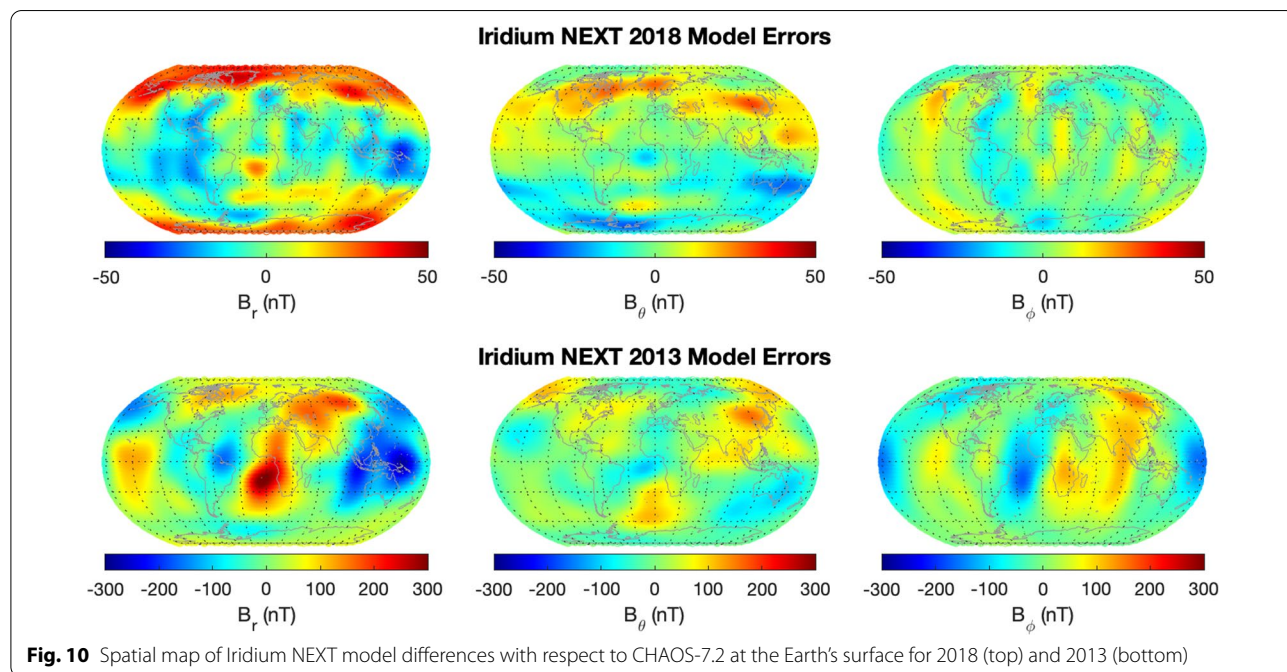
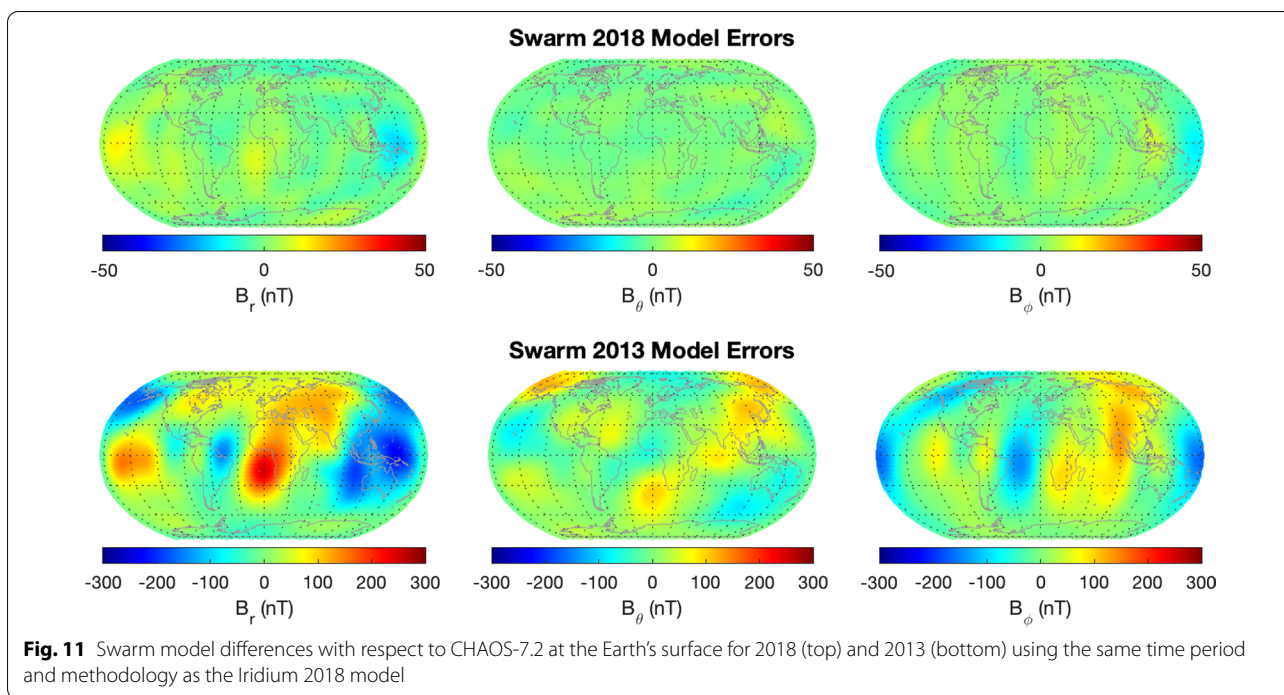


Fig. 10 Spatial map of Iridium NEXT model differences with respect to CHAOS-7.2 at the Earth’s surface for 2018 (top) and 2013 (bottom)



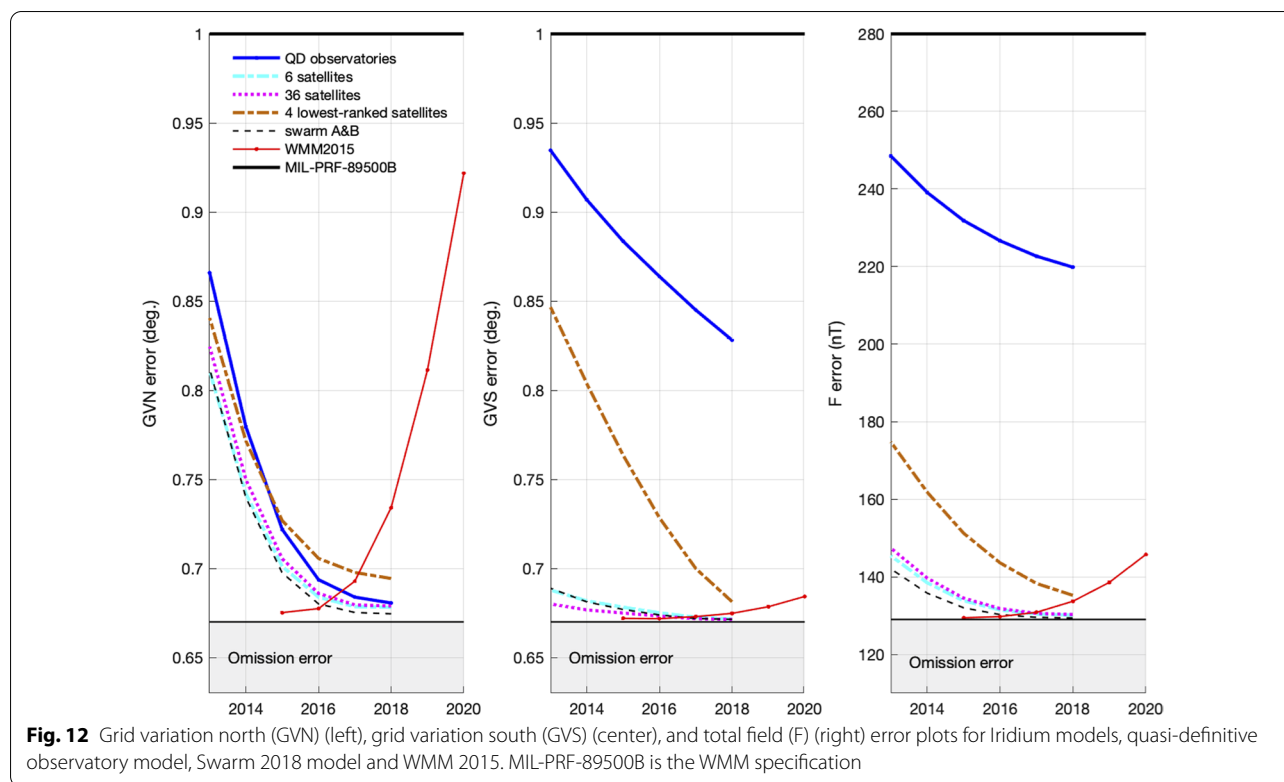
dependence, which suggests that these errors are driven by measurement errors and sampling, rather than the calibration. A summary of the model residuals is provided in Table 1.

The model errors in 2013 are shown in the bottom panels of Fig. 10. By the end of the 5-year model interval, the maximum errors increased from 40 nT to >300 nT, and the average error increased from 20 nT to 125 nT. The errors in 2013 are dominated by nonlinear changes in the core field between 2013 and 2018, rather than errors in the Iridium model at the 2018 epoch. This is supported by similar results from a Swarm 2018 model introduced below.

It is an interesting and positive result that the large errors in the quasi-definitive observatory model do not fully translate into the Iridium model through the calibration. The Iridium spacecraft attitude is nominally defined by pointing the Z axis toward nadir and the Y axis anti-aligned the orbit normal vector. This causes the linear calibration, which is fixed to the spacecraft frame, to have a regular mapping to latitude. The high-inclination orbit allows all longitudes to be sampled each day, so the longitudinal coupling is reduced through daily calibrations. The coupling between calibration parameters and the model is strongest in the lower order terms: for example, a scale factor error can alter the magnitude of the main field dipole term while preserving the directional features

of the field, and a bias error along the nadir-pointing spacecraft axis produces a sinusoidal error with latitude in the model. The coupling between the reference model used for calibration and the calibration parameters is complicated and depends on the spacecraft pointing mode and the spatial distribution of reference model errors. Through empirical tests, we found that the calibration parameters become relatively insensitive to reference model terms above SH degree 8.

We produced a 2018 main field model with Swarm data to better understand the effect of Iridium measurement errors on the model, as the Swarm measurements are much more accurate (~1 nT). The Swarm model uses the same data interval and modeling assumptions as the Iridium model. We found that the Swarm model did not require regularization to reasonably match the CHAOS secular variation spectrum up to SH degree 12. We attribute this to the fact that Swarm provides global low-noise coverage of the geomagnetic field as well as our use of linear Gauss coefficients during the 14-month model interval. Longer period geomagnetic models, such as CHAOS, typically use higher order splines to model temporal changes that need to be regularized to avoid unphysically large oscillations in the splines, which is not the case for our model. The 2018 model errors in Fig. 11 (top panels) reflect the influence of modeling



assumptions, such as quiet-time data selection, external field subtraction, linear secular variation, and the data interval. The WMM is typically derived from 3 years of data, but only 14 months of Iridium data were available for this study. The Swarm model has ~ 5 – 15 nT errors at the 2018 model epoch, and the errors are slightly larger in the B_r component than the B_θ and B_ϕ components. Larger radial errors were also present in the Iridium model. Some of the Swarm model error may be related to using data from a single orbital plane, which causes data gaps as the orbit precesses through the nightside local time region used for main field modeling.

When evaluated in 2013, the Swarm model exhibits similar error patterns as the Iridium model [Fig. 11 (bottom panels)], indicating that these errors primarily reflect nonlinear changes in the core field between 2013 and 2018, rather than errors specific to the Iridium model. There was a geomagnetic jerk in 2014 (Torta et al. 2015) and a secular acceleration pulse in 2016–2017 (Alken et al. 2020), which causes the 2018 models to deviate when extrapolated to 2013 using a constant secular variation term. This demonstrates that the model uncertainty due to Iridium measurement errors is small compared to the natural variability of the core field over the 5-year model interval.

WMM error evaluation

The primary motivation of this study was to determine whether Iridium data could be used to make future WMMs after the Swarm era. The WMM has requirements on model accuracy in terms of global root-mean square error in total field, declination, inclination, horizontal intensity, and grid variation that must be satisfied over the 5-year interval of the model (Chulliat et al. 2020). Grid variation is defined as the difference between declination and longitude above 55° and below -55° latitudes. (It is an example of a more general concept, also called “grivation”, which is the angle between grid north on a map and magnetic north. We use the term “grid variation” here, because it is the one used in the WMM specification; see Department of Defense, 2019). Grid variation error is effectively high-latitude declination error computed separately for the northern and southern hemispheres above 55° latitude. Figure 12 compares the grid variation north (GVN), grid variation south (GVS), and total field (F) errors for several models. This error is obtained by adding (in an RMS sense) (a) the omission error associated with unmodeled sources (e.g., magnetized rocks, electric currents outside the Earth), which is assumed constant in time, and (b) the time-varying core field error. The values for the omission error are provided in Chulliat et al. (2020, Table 15). The error is typically small at the

model epoch, and grows over time due to errors in the linear secular variation estimate and real non-linear changes in the core field. The 2018 models were evaluated backward in time to compare to existing data, and the 2015 WMM was evaluated forward in time from the 2015 epoch. The quasi-definitive observatory model is derived with limited observations in the southern hemisphere, which causes larger errors in the GVS and total field plots. There is a significant improvement in the error for Iridium-based models, highlighting the benefit of full global sampling by the constellation. The 6-satellite Iridium model based on the spacecraft with the lowest residual ranking from each orbital plane performs similarly to the model that incorporates all 36 Iridium satellites. To illustrate the impact of selecting satellites with different residual characteristics, we constructed a model with the four lowest ranked satellites (SV159, SV180, SV167, SV171). Although this model meets WMM requirements, the errors are distinctly larger than the other Iridium models, indicating that there may be an advantage to identifying and removing spacecraft with larger residuals from future models. From a WMM perspective, the 6- and 36-satellite Iridium models perform similarly to the WMM 2015 and the 2018 Swarm model, demonstrating that Iridium is a viable solution for future WMMs.

Effect of increasing number of satellites

In Fig. 13, we explore the effect of increasing the number of satellites on the model accuracy expressed in terms of vector error. Vector error is a global average of the error in the model at the surface of the Earth, and it is computed by taking the square root of the sum of the model error power up to SH degree 12 (Alken et al. 2021a, Eq. 5). CHAOS-7.2 was used for the reference model, and the vector error was evaluated at 2018.

For models with 6 or fewer satellites, combinations of the 6 best satellites from each orbital plane were selected. The 2-satellite models use spacecraft from orthogonal planes, and the 3-satellite models have 60° separation between orbital planes. Above 6 satellites, progressively lower ranked satellites were added to each plane when available. One plane has only a single satellite, and another plane has 2 satellites. The satellites used in each model are listed in Table 2.

There is considerable variation in the vector error when only a single satellite is included in the model. We attribute this variation to irregular temporal sampling during the 14-month modeling interval. The model only uses data when the orbital plane precesses through local times between 22:00 and 05:00, so the single-plane models include less data for averaging both random errors and

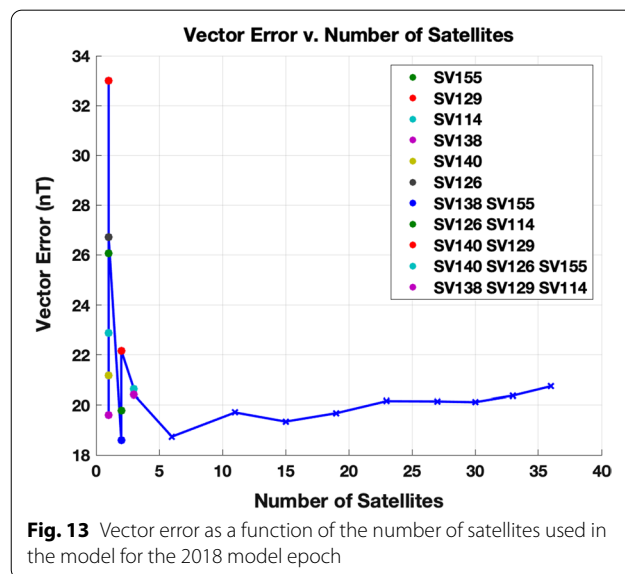


Fig. 13 Vector error as a function of the number of satellites used in the model for the 2018 model epoch

Table 2 Iridium NEXT Residual Ranking by Orbit Plane

Number of satellites	Plane 1	Plane 2	Plane 3	Plane 4	Plane 5	Plane 6
6	SV140	SV138	SV126	SV129	SV155	SV114
11	SV144	SV113	SV168		SV154	SV112
15	SV146		SV172		SV156	SV102
19	SV148		SV180		SV166	SV106
23	SV149		SV167		SV165	SV104
27	SV145		SV171		SV158	SV103
30	SV150				SV160	SV111
33	SV157				SV163	SV147
36	SV153				SV159	SV152

seasonal variations in external fields. As data from additional planes are included, the vector error decreases, with a minimum when the best spacecraft is selected from each of the 6 planes. There is a gradual non-monotonic increase in error as more spacecraft with larger residuals are added, indicating that the advantage of averaging more data is offset by including lower quality measurements. The 36 satellites available for this study are not evenly distributed among the 6 orbital planes and the residual statistics vary between planes. This may cause the non-monotonic increase in vector error in models with more than 6 satellites.

For this initial study, the spacecraft were ranked using residuals relative to CHAOS-7.2, which depends on Swarm data. Since the Swarm mission currently overlaps with Iridium, we plan to use the CHAOS ranking as a starting point for selecting satellites. We experimented with ranking the satellites relative to a model derived from all 36 Iridium satellites as a solution to assessing measurement quality after the Swarm mission ends, and while the ranking was not identical to the CHAOS ranking, the four satellites with the largest residuals were correctly identified with this method. This result indicates that we can monitor measurement degradation in the future without depending on Swarm.

Conclusions

This study explored the feasibility of producing main field models using Iridium NEXT magnetometer data. Due to a lack of an onboard absolute scalar magnetometer, the fluxgate measurements cannot be independently calibrated, and the factory calibration results in large (>1000 nT) errors. After calibration relative to the CHAOS model, the Iridium residuals were significantly reduced, with typical standard deviations of 20–40 nT.

To produce Iridium models that are independent of data from a Swarm-like scientific spacecraft, we calibrated the data relative to a main field model based on measurements from 59 observatories producing quasi-definitive data on a regular basis. Although the quasi-definitive observatory model contained large (~500 nT) errors due to insufficient spatial sampling, only a fraction of these errors propagated into the Iridium data through the calibration process. Models developed with calibrated

Iridium data had maximum errors of ~40 nT and globally averaged errors of ~20 nT. For comparison, a Swarm model using the same modeling assumptions had maximum errors of ~15 nT and globally averaged errors of ~6 nT. At the model epoch, Iridium-based models are expected to have slightly larger errors (~15 nT rms) than recent versions of the WMM, however, the secular variation uncertainty and non-linear variation in the core field quickly become the dominant error source as time progresses from the epoch.

Models using various combinations of spacecraft from the Iridium constellation were evaluated to explore the effect of including data from additional orbital planes and data from spacecraft with larger residuals. The results showed that the models improve as the number of orbital planes are increased, with a minimum error for the model using the satellite with the lowest residuals from each of the 6 orbital planes. Using all 6 orbital planes allows for continuous sampling in the nighttime sector used for main field modeling, whereas a single orbital plane has temporal gaps due to orbital precession. Adding additional satellites with larger residuals to the models generally increased the overall error, demonstrating that the advantages of averaging more data were offset by including additional lower quality data.

The Iridium NEXT models were shown to meet WMM accuracy requirements over a 5-year interval for the 2018 model epoch, and the performance relative to WMM specifications was comparable to the WMM 2015 and the 2018 Swarm model. There are many scientific applications that require Swarm-like magnetometer measurements, so Iridium should not be viewed as an equivalent replacement for Swarm. However, this study demonstrates that the Iridium NEXT data offer a viable alternative to highly accurate scientific data for future operational main field models. Although Iridium data are not currently available to the public, the results of this study show more broadly that lower quality magnetometer data can be used to construct main field reference models, such as the WMM. Given the recent increase in launches of commercial satellite constellations, these types of data sets will likely become more common in the future, offering a potentially valuable data source for the scientific community.

Table 3 Quasi-definitive observatories used for calibration model, including estimated crustal biases which are given in units of nT

IGAA code	Name	Country	Colatitude (°)	East longitude (°)	Bias B_r	Bias B_θ	Bias B_ϕ	Data start	Data end
ABK	Abisko	Sweden	21.642	18.823	- 28.3	- 21.2	57.5	1 Jan 1998	31 Jul 2020
ASC	Ascension Island	United Kingdom	97.95	345.62	- 25.8	497.7	269.4	1 Jan 1998	21 Jul 2020
ASP	Alice Springs	Australia	113.77	133.88	- 40.6	- 53.2	- 19.2	1 Jan 1998	30 Jun 2020
BEL	Belsk	Poland	38.164	20.789	- 311.7	- 127.0	135.3	1 Jan 1998	30 Jun 2020
BOU	Boulder	United States of America	49.86	254.76	139.2	- 0.9	37.6	1 Jan 1998	30 Jun 2020
BOX	Borok	Russia	31.93	38.23	349.8	- 2.6	1.8	1 Jan 1998	30 Apr 2020
BRW	Barrow	United States of America	18.68	203.38	53.0	- 34.9	- 67.0	2 Jan 1998	30 Jun 2020
CKI	Cocos-Keeling Islands	Australia	102.1875	96.8336	169.6	259.2	- 97.2	1 Jan 2013	30 Jun 2020
CLF	Chambon la Foret	France	41.98	2.27	- 107.0	65.7	- 16.0	1 Jan 1998	30 Apr 2020
CMO	College	United States of America	25.13	212.14	11.9	- 17.4	8.5	1 Jan 1998	30 Jun 2020
CNB	Canberra	Australia	125.32	149.36	- 78.7	- 3.8	49.0	1 Jan 1998	30 Jun 2020
CSY	Casey Station	Antarctica	156.283	110.533	408.1	- 720.1	- 169.5	1 Jan 2011	31 May 2020
CTA	Charters Towers	Australia	110.1	146.3	- 176.1	437.6	- 83.9	1 Jan 1998	30 Jun 2020
CYG	Cheongyang	Republic of Korea	53.63	126.854	97.2	50.1	52.7	1 Jan 2014	14 Dec 2019
DLT	Dalat	Vietnam	78.06	108.48	- 137.6	56.5	- 44.8	20 Apr 2011	28 Dec 2019
DOU	Dourbes	Belgium	39.9	4.6	- 77.5	- 25.3	- 18.0	1 Jan 1998	31 May 2020
EBR	Ebro	Spain	49.043	0.333	- 4.9	1.5	5.4	1 Jan 1998	31 May 2020
ESK	Eskdalemuir	United Kingdom	34.68	356.8	60.1	- 20.2	- 34.6	1 Jan 1998	21 Jul 2020
FRD	Fredericksburg	United States of America	51.8	282.63	- 110.6	- 83.2	- 44.4	1 Jan 1998	30 Jun 2020
FRN	Fresno	United States of America	52.91	240.28	235.7	- 5.4	- 16.9	1 Jan 1998	30 Jun 2020
GNG	Gingin	Australia	121.356	115.715	- 164.8	- 0.9	- 38.5	1 Jan 2012	30 Jun 2020
GUA	Guam	United States of America	76.41	144.87	- 54.2	- 126.1	78.9	2 Jan 1998	30 Jun 2020
HAD	Hartland	United Kingdom	39	355.52	- 67.5	31.7	14.6	1 Jan 1998	21 Jul 2020
HER	Hermanus	South Africa	124.43	19.23	- 26.3	- 29.5	7.3	1 Jan 1998	31 Jul 2020
HON	Honolulu	United States of America	68.68	202.0	324.2	162.0	88.8	1 Jan 1998	3 Feb 2020
HRN	Hornsund	Norway	12.998	15.547	44.3	30.5	- 49.1	1 Jan 1998	30 Jun 2020
HYB	Hyderabad	India	72.6	78.6	- 468.3	- 270.5	26.8	1 Jan 2009	6 Jul 2020
JCO	Jim Carrigan Observatory	United States of America	19.644	211.201	49.5	13.2	- 40.9	1 Jan 2005	21 Jul 2020
KAK	Kakioka	Japan	53.77	140.18	98.0	- 14.3	14.4	1 Jan 1998	31 May 2020
KDU	Kakadu	Australia	102.69	132.47	- 20.8	- 11.3	- 33.0	1 May 1998	30 Jun 2020
KEP	King Edward Point	South Georgia and the South Sandwich Islands	144.2821	323.5071	- 86.6	26.6	- 44.2	25 Feb 2011	21 Jul 2020
KHB	Khabarovsk	Russia	42.39	134.69	- 606.8	281.0	- 429.3	1 Jan 2012	23 Jul 2020
KNY	Kanoya	Japan	58.58	130.88	39.4	- 4.4	52.4	1 Jan 1998	31 May 2020
KOU	Kourou	French Guiana	84.79	307.27	39.7	- 112.6	99.8	12 Jan 1998	30 Apr 2020
LER	Lerwick	United Kingdom	29.87	358.82	- 40.1	126.2	175.9	1 Jan 1998	21 Jul 2020
LRM	Learmonth	Australia	112.22	114.1	- 173.7	28.8	- 33.0	1 Jan 1998	30 Jun 2020
LYC	Lycksele	Sweden	25.4	18.8	212.9	- 134.6	- 34.6	1 Jan 2008	31 Jul 2020
MAW	Mawson	Antarctica	157.6	62.88	- 184.7	- 44.1	6.3	1 Jan 1998	30 Jun 2020
MCQ	Macquarie Island	Australia	144.5	158.95	- 291.4	- 278.4	- 2.6	1 Jan 1998	30 Jun 2020
MGD	Magadan	Russia	29.949	150.728	- 44.6	251.1	- 718.4	1 Jan 2012	12 Jul 2020
MMB	Memambetsu	Japan	46.09	144.19	- 47.1	207.2	144.4	1 Jan 1998	31 May 2020

Table 3 (continued)

IGA code	Name	Country	Colatitude (°)	East longitude (°)	Bias B_r	Bias B_θ	Bias B_ϕ	Data start	Data end
NAQ	Narsarsuaq	Greenland	28.84	314.558	− 466.1	288.8	266.5	1 Jan 1998	31 May 2020
NEW	Newport	United States of America	41.73	242.88	125.2	20.5	114.9	1 Jan 1998	30 Jun 2020
NGK	Niemegk	Germany	37.93	12.68	78.1	12.3	− 0.8	1 Jan 1998	30 Jul 2020
NVS	Novosibirsk	Russia	35.15	83.23	− 18.7	− 77.6	− 55.1	1 Jan 1998	26 Jul 2020
PET	Paratunka	Russia	37.029	158.248	− 134.4	293.3	251.8	1 Jan 1998	25 Jul 2020
PST	Port Stanley	Falkland Islands	141.7	302.11	− 32.3	− 36.1	− 11.5	7 Sep 2005	21 Jul 2020
SBL	Sable Island	Canada	46.0679	299.9905	88.6	− 11.5	9.3	1 Jan 2000	21 Jul 2020
SFS	San Fernando	Spain	53.333	354.055	− 153.0	93.4	31.9	1 Jan 1998	30 Jul 2020
SHU	Shumagin	United States of America	34.65	199.54	− 29.5	− 415.9	− 234.4	1 Jan 2005	25 Jun 2020
SIT	Sitka	United States of America	32.94	224.67	85.6	− 27.2	− 16.0	1 Jan 1998	30 Jun 2020
SJG	San Juan	United States of America	71.89	293.85	− 127.2	51.6	131.3	1 Jan 1998	30 Jun 2020
SPT	San Pablo-Toledo	Spain	50.45	355.65	26.9	− 13.7	9.1	1 Jan 1998	31 May 2020
TAM	Tamanrasset	Algeria	67.21	5.53	59.0	− 56.5	− 218.8	1 Jan 1998	30 Apr 2020
THY	Tihany	Hungary	43.1	17.89	57.3	5.5	− 12.9	1 Jan 1999	31 Dec 2018
TUC	Tucson	United States of America	57.82	249.27	− 419.5	82.0	− 265.2	1 Jan 1998	30 Jun 2020
UPS	Uppsala	Sweden	30.097	17.353	119.9	− 151.9	− 14.5	1 Jan 2003	31 Jul 2020
WIC	Conrad Observatory	Austria	42.0695	15.8657	18.3	− 14.9	− 2.5	1 Jan 2015	24 Jul 2020
WNG	Wingst	Germany	36.26	9.07	73.4	− 68.0	49.0	1 Jan 1998	30 Jul 2020

The last two columns provide the time period of data availability used to estimate the crustal biases

Appendix A: Quasi-definitive observatories

Acknowledgements

We thank the National Geospatial-Intelligence Agency WMM team for supporting this study. The European Space Agency is gratefully acknowledged for providing Swarm data. The results presented in this paper rely on data collected at magnetic observatories. We thank the national institutes that support them and INTERMAGNET for promoting high standards of magnetic observatory practice (<http://www.intermagnet.org>).

Authors' contributions

SC analyzed raw Iridium data, calibrated the spacecraft data, produced the Iridium main field models, and is the primary author. PA developed the quasi-definitive observatory model and the main field inversion software. AC analyzed the models relative to the WMM specifications. SC, PA and AC designed the study. BA, KR, SV, RB and KL applied corrections for spacecraft contamination and provided processed Iridium data to the University of Colorado at Boulder for this study. All authors discussed the results and contributed to the writing of the manuscript. All authors read and approved the final manuscript.

Funding

This research was supported by the NOAA Cooperative Agreement with CIRES, NA17OAR4320101. Support for acquisition and calibration analysis of data from Iridium NEXT was provided by NSF for AMPERE under Grants AGS-1420184 and AGS-2002574.

Availability of data and materials

The University of Colorado Boulder obtained the Iridium data for this study under a license agreement. At present, the Iridium data set is not publicly available. INTERMAGNET data are available at <http://www.intermagnet.org>. Swarm data are available from <https://earth.esa.int/web/guest>.

Declarations

Competing interests

The authors declare that they have no competing interests.

Author details

¹Cooperative Institute for Research in Environmental Sciences, University of Colorado, Boulder, USA. ²National Centers for Environmental Information, Boulder, USA. ³The Johns Hopkins Applied Physics Laboratory, Laurel, USA. ⁴Iridium Satellite LLC, Leesburg, USA.

Received: 24 May 2021 Accepted: 6 January 2022

Published online: 25 February 2022

References

- Alken P, Olsen N, Finlay CC (2020) Co-estimation of geomagnetic field and in-orbit fluxgate magnetometer calibration parameters. *Earth Planets Space* 72:1–32
- Alken P, Thebault E, Beggan C, Aubert J, Baerenzung J, Brown WJ, Califf S, Chulliat A, Cox G, Finlay CC et al (2021) Evaluation of candidate models for the 13th generation international geomagnetic reference field. *Earth Planet Space* 73(1):1–21. <https://doi.org/10.1186/s40623-020-01281-4>
- Alken P, Thebault E, Beggan CD, Amit H, Aubert J, Baerenzung J, Bondar T, Brown W, Califf S, Chambodut A et al (2021) International geomagnetic reference field: the thirteenth generation. *Earth Planet Space* 73(1):1–25. <https://doi.org/10.1186/s40623-020-01288-x>

- Anderson BJ, Takahashi K, Toth BA (2000) Sensing global birkeland currents with iridium[®] engineering magnetometer data. *Geophys Res Lett* 27(24):4045–4048
- Anderson BJ, Angappan R, Barik A, Vines SK, Stanley S, Bernasconi PN, Korth H, Barnes RJ (2021) Iridium communications satellite constellation data for study of earth's magnetic field. *Geochem Geophys Geosy* 22(8):e2020GC009515
- Chulliat A, Brown W, Alken P, Beggan C, Nair M, Cox G, Woods A, Macmillan S, Meyer B, Panizza M (2020) The US/UK World Magnetic Model for 2020–2025: Technical Report. National Centers for Environmental Information, NOAA. <https://doi.org/10.25923/ytk1-yx35>
- Chulliat A, Brown W, Alken P, Macmillan S, Panizza M (2021) Modeling Earth's ever-shifting magnetism. *Eos*, p 102. <https://doi.org/10.1029/2021EO153457>
- Finlay CC, Kloss C, Olsen N, Hammer MD, Tøffner-Clausen L, Grayver A, Kuvshinov A (2020) The CHAOS-7 geomagnetic field model and observed changes in the South Atlantic Anomaly. *Earth Planet Space* 72(1):1–31. <https://doi.org/10.1186/s40623-020-01252-9>
- Friis-Christensen E, Lühr H, Hulot G, (2006) Swarm: a constellation to study the earth's magnetic field. *Earth Planet Space* 58:351–358. <https://doi.org/10.1186/BF03351933>
- Hansen PC, O'Leary DP (1993) The use of the I-curve in the regularization of discrete ill-posed problems. *SIAM J Sci Comput* 14(6):1487–1503
- Hapgood M (1992) Space physics coordinate transformations: a user guide. *Plane Space Sci* 40(5):711–717. [https://doi.org/10.1016/0032-0633\(92\)90012-D](https://doi.org/10.1016/0032-0633(92)90012-D). <https://www.sciencedirect.com/science/article/pii/003206339290012D>
- Lowes FJ (1966) Mean-square values on sphere of spherical harmonic vector fields. *J Geophys Res* 71(8):2179–2179. <https://doi.org/10.1029/JZ071i008p02179>
- Lowes FJ, (1974) Spatial power spectrum of the main geomagnetic field, and extrapolation to the core. *Geophys J Int* 36(3):717–730. <https://doi.org/10.1111/j.1365-246X.1974.tb00622.x>
- Macmillan S, Olsen N (2013) Observatory data and the swarm mission. *Earth Planet Space* 65(11):15. <https://doi.org/10.5047/eps.2013.07.011>
- Maus S, Yin F, Lühr H, Manoj C, Rother M, Rauberg J, Michaelis I, Stolle C, Müller R (2008) Resolution of direction of oceanic magnetic lineations by the sixth-generation lithospheric magnetic field model from champ satellite magnetic measurements. *Geochemistry, Geophysics, Geosystems* 9(7):1
- Olsen N, Clausen LT, Sabaka TJ, Brauer P, Merayo JM, Jørgensen JL, Léger J-M, Nielsen OV, Primdahl F, Risbo T (2003) Calibration of the ørsted vector magnetometer. *Earth Planet Space* 55(1):11–18. <https://doi.org/10.1186/BF03352458>
- Olsen N, Lühr H, Finlay CC, Sabaka TJ, Michaelis I, Rauberg J, Tøffner-Clausen L (2014) The CHAOS-4 geomagnetic field model. *Geophys J Int* 197(2):815–827
- Peltier A, Chulliat A (2010) On the feasibility of promptly producing quasi-definitive magnetic observatory data. *Earth Planet Space* 62(2):e5–e8. <https://doi.org/10.5047/eps.2010.02.002>
- Performance specification - World Magnetic Model (WMM), Doc. MIL-PRF-89500B. Natl. Geospatial-Intell. Agency, Department of Defense. Arlington, Va., 2019. http://everyspec.com/MIL-PRF/MIL-PRF-080000-99999/MIL-PRF-89500B_56010/
- Richmond A (1995) Ionospheric electrodynamic using magnetic apex coordinates. *J Geomagn Geoelectr* 47:01. <https://doi.org/10.5636/jgg.47.191>
- Shure L, Parker RL, Backus GE (1982) Harmonic splines for geomagnetic modeling. *Phys Earth Planet Inter* 28(3):215–229
- Smith W, Wessel P (1990) Gridding with continuous curvature splines in tension. *Geophysics* 55(3):293–305
- Tøffner-Clausen L, Lesur V, Olsen N, Finlay CC (2016) In-flight scalar calibration and characterisation of the Swarm magnetometry package. *Earth Planet Space* 68(1):1–13. <https://doi.org/10.1186/s40623-016-0501-6>
- Torta JM, Pavón-Carrasco FJ, Marsal S, Finlay CC (2015) Evidence for a new geomagnetic jerk in 2014. *Geophys Res Lett* 42(19):7933–7940
- Verbanac G, Mandea M, Bandić M, Subašić S (2015) Magnetic observatories: biases over CHAMP satellite mission. *Solid Earth* 6(2):775–781

Publisher's Note

Springer Nature remains neutral with regard to jurisdictional claims in published maps and institutional affiliations.

Submit your manuscript to a SpringerOpen[®] journal and benefit from:

- Convenient online submission
- Rigorous peer review
- Open access: articles freely available online
- High visibility within the field
- Retaining the copyright to your article

Submit your next manuscript at ► [springeropen.com](https://www.springeropen.com)